The Cryosphere Discuss., 2, 487–511, 2008
www.the-cryosphere-discuss.net/2/487/2008/

The Cryosphere Discussions

The Cryosphere Discussions is the access reviewed discussion forum of *The Cryosphere*

On the use of incoming longwave radiation parameterizations in a glacier environment

J. Sedlar[1] **and R. Hock**[2,3]

[1]Department of Meteorology, Stockholm University, Sweden
[2]Geophysical Institute, University of Alaska Fairbanks, USA
[3]Department of Earth Sciences, Uppsala University, Sweden

Received: 7 May 2008 – Accepted: 19 May 2008 – Published: 1 July 2008

Correspondence to: J. Sedlar (josephs@misu.su.se)

Published by Copernicus Publications on behalf of the European Geosciences Union.

Abstract

Energy balance based glacier melt models require accurate estimates of incoming longwave radiation since it is generally the largest source of energy input. Multi-year near-surface meteorological data from Storglaciären, northern Sweden, were used to evaluate commonly used longwave radiation parameterizations in a glacier environment under clear-sky, overcast-sky and all-sky conditions. The tested parameterization depending solely on air temperature performed worse than those including also air humidity. Adopting parameter values from the literature instead of fitting them to the data resulted in similar correlation coefficients between modeled and measured radiation, but generated larger biases, emphasizing the need to derive site-specific coefficients. Nearly all models including those fitted to the data tended to overestimate longwave radiation during periods of low longwave radiation, and vice versa when radiation input was high. An attempt was made to parameterize cloud cover using top of atmosphere and measured global radiation. Both hourly and daily calculations of incoming longwave radiation using the cloud parameterization provided similar, or even stronger, correlations to the measurements compared to using observed cloud fraction as input. Using the global radiation cloud parameterization is promising for use in high-latitude regions where global radiation measurements exist but cloud observations do not.

1 Introduction

Energy balance studies on glaciers have shown that on average net radiation usually is the largest contributor to surface ice and snow melt (see summary in Hock and Holmgren, 2005). Examination of the individual radiation components reveals that longwave incoming radiation (also referred to as downward or downwelling longwave radiation or atmospheric radiation) is by far the largest source of energy for melt, followed by absorbed global (or shortwave) radiation (Ohmura, 2001) which only accounts for roughly a quarter of the total heat source. Sensible heat flux provides usually the third largest

TCD
2, 487–511, 2008

energy source. In light of a changing climate, the importance of longwave incoming radiation may increase (Philipona et al., 2004). Hence, its accurate modeling is of paramount importance in energy balance glacier melt modeling and assessing the response of glacier melt to climate warming.

Longwave radiation fluxes have generally received less attention than shortwave fluxes, partially due to difficulties and costs associated with accurate longwave radiation measurements and also due to a void of measurable atmospheric parameters which longwave radiation is dependent upon, such as cloud cover (Aase and Idso, 1978; Müller, 1985; Marty and Philipona, 2000). Unlike global radiation (shortwave incoming radiation), incoming longwave radiation is not readily measured at automated weather stations, often being derived through combination of global and net radiation measurements or parameterizations, although the number of weather stations on glaciers equipped with longwave radiation instrumentation has increased during recent years (e.g. van den Broeke et al., 2004; Sicart et al., 2005; van de Wal et al., 2005; Hoch et al., 2007).

The atmospheric flux of longwave radiation is emitted predominantly by clouds, water vapor, carbon dioxide and ozone. The flux varies mostly with the amount and temperature of cloud cover and water vapor, and because of the temperature dependence generally decreases with increasing altitude (Marty et al., 2002). In mountain areas longwave irradiance from the surrounding terrain may locally enhance irradiance and thus generate spatial variability in melt (Plüss and Ohmura, 1997; Sicart et al., 2006). Ideally the longwave radiation flux is modeled with physical models describing all emission and absorption processes in the atmosphere. However, such models are not applicable when vertical profile data of temperature and moisture are lacking. Hence, empirical relationships have been developed parameterizing longwave incoming radiation as a function of near-surface (e.g. 2 m) temperature and/or vapor pressure for clear-sky conditions, and in addition as a function of cloud cover fraction in case of all-sky conditions. Use of standard meteorological measurements at near surface level has proven sufficient since most incoming longwave radiation reaching the Earth's sur-

face is emitted from the lowest layers of the troposphere (Ohmura, 2001). Only few studies have compared different parameterizations on the same data set (e.g. Sugitia and Brutsaert, 1993; Pirazzini et al., 2000, 2001; Gabuthuler et al., 2001; Iziomon et al., 2003) and most studies have focused on lowland station data. Also, much attention has been devoted to clear-sky longwave radiation, although cloudy conditions often prevail in mountain and glacier environments.

The purpose of this study is to evaluate and compare various commonly used parameterizations of longwave incoming radiation in a glacier environment. The parameterizations include screen-level air temperature, water vapor pressure and cloud cover fraction as independent variables. Secondly, we develop a new parameterization for cloud cover since existing models often use cloud cover as dependent variable, but such observations tend to be scarce in a glacier environment. We parameterize cloud cover fraction as a function of global radiation and top of atmosphere radiation, and incorporate this parameterization into the calculations of longwave incoming radiation. Our analysis is based on a detailed micrometeorological data set collected on Storglaciären, a small glacier in northern Sweden, during four melt seasons.

2 Site description and data

Storglaciären is located in Northern Sweden (67°55′ N, 18°35′ E) comprising an area of ∼3 km^2. Elevation ranges between 1120–1730 m a.s.l. Mean summer temperature (June–August 1965–2003) at Tarfala Research Station located ∼1 km from the glacier is −3.7°C (Radic and Hock, 2006). An automatic weather station was operated in the upper region of the ablation zone at approximately 1390 m a.s.l. during the 1998–2000 and 2002 melt seasons. A detailed description of measurements and instrumentation is found in Hock et al. (1999); important to this study are incoming longwave radiation, global radiation, near-surface air temperature and humidity and cloud fraction.

An Eppley Precision Infrared Radiometer was used to measure incoming longwave radiation. The instrument underwent "Swiss modification" at the World Radiation Cen-

ter in Davos, Switzerland, which incorporates three dome thermistors separated by 120° and an elevation of 45°, rather than using a single thermistor as in the original instrument. Details are given in Philipona et al. (1995) who claim that the accuracy of the modified instrument is 2 W m^{-2} compared to approximately 10 W m^{-2} of the unmodified version. Global radiation was measured by a Kipp & Zonen CM11 with a reported maximum uncertainty of 2% for hourly values; temperature and humidity were measured by a Vaisala HMP45D. This instrument reports temperature accuracy of ±0.3°C at 0°C; humidity accuracy is reported as ±3% (0<RH<90%) and ±4% (90<RH<100%) at 0°C. Temperature and humidity measurements were maintained at 2 m heights, while radiation measurements varied in height between 1–1.5 m above the glacier surface. All instruments mentioned above were artificially ventilated to reduce measurement errors. Measurements were taken every 60 s and hourly means were stored on a data logger. The weather station was visited at least twice a week for most of the melt seasons. Manual sky observations were recorded by trained observers in the vicinity of the automatic weather station. Hourly cloud observations were performed, including cloud fraction and cloud-base level classified into three levels (high, middle, low).

3 Parameterizations and methods

Incoming longwave radiation, $L\downarrow$ (W m^{-2}) is generally expressed in terms of the Stefan-Boltzmann Law

$$L\downarrow = \varepsilon_{\text{eff}}\sigma T^4 = \varepsilon_{cs} F \sigma T^4 \quad (1)$$

where $\varepsilon_{\text{eff}}=\varepsilon_{cs}F$ is referred to as the effective or apparent emissivity (Unsworth and Monteith, 1975) and generally varies between roughly 0.7 for clear skies to close to unity for completely overcast skies. ε_{cs} is the clear-sky atmospheric emissivity. F (always ≥1) is a cloud factor expressing the increase in clear-sky $L\downarrow$ due to cloud emission, σ is the Stefan-Boltzmann constant (5.67×10^{-8} W m^{-2} K^{-4}) and T is the absolute temperature (K) at the reference height (here 2 m). Parameterizations of clear-sky

and effective emissivity have been developed both theoretically and empirically (e.g. Ångström, 1916; Brunt, 1932; Swinbank, 1963; Brutsaert, 1975; Yamannouchi and Kawaguchi, 1984; Konzelmann et al., 1994). This study focuses on the parameterizations proposed by Idso and Jackson (1969), Brutsaert (1975) and Konzelmann et al. (1994).

3.1 Clear-sky conditions (F=1)

Idso and Jackson (1969) expressed clear-sky emissivity ε_{cs} as a function of near-surface temperature T_a (K):

$$\varepsilon_{cs}(T_a) = 1 - 0.261 \exp\left[-7.77 \times 10^{-4} \cdot (273 - T_a)\right]. \quad (2)$$

The constants were determined theoretically using standard atmosphere assumptions. We choose this model as a "building block" example, based solely on air temperature as independent variable. Brutsaert's (1975) model, which is widely used for clear-sky $L\downarrow$ computations, includes near-surface vapor pressure e_a (Pa) as a second input variable

$$\varepsilon_{cs}(e_a, T_a) = k \left(\frac{e_a}{T_a}\right)^{\frac{1}{m}} \quad (3)$$

where k and m are coefficients determined as 0.642 and 7, respectively, by Brutsaert (1975). Brutsaert's (1975) Eq. (3), like Idso and Jackson's (1969) Eq. (2), was theoretically derived assuming standard atmosphere conditions.

Finally, the clear-sky equation by Konzelmann et al. (1994) was used

$$\varepsilon_{cs}(e_a, T_a) = 0.23 + b \left(\frac{e_a}{T_a}\right)^{\frac{1}{m}} \quad (4)$$

which is a modified version of Brutsaert's (1975) Eq. (3). Konzelmann et al. (1994) included the addition of 0.23 to account for the emissivity of a completely dry atmosphere as calculated by a numerical radiation model, and thus in contrast to Brutsaert

(1975), can account for greenhouse gases other than water vapor. Coefficients b and m were obtained empirically to hourly and daily mean data from the ETH camp in West Greenland (Konzelmann et al., 1994).

Equations (2) and (3) were chosen to identify any improvements in $L\downarrow$ calculations when a measure of water vapor is included in the calculations. Equation (4) was chosen because it was empirically developed from measurements in a glacier environment and has been widely used in glacier studies (Zuo and Oerlemans, 1996; van den Broeke, 1996; Greuell et al., 1997; Klok and Oerlemans, 2002). Clear-sky emissivity values were computed ($\varepsilon_{cs}=L\downarrow/\sigma T^4$) from all hourly data of $L\downarrow$ and T from Storglaciären when cloud cover fraction $n\leq 1/8$ (N=205), and then related to e/T to determine the coefficients in Eq. (4) through robust fitting, a technique that assumes a least-squares fit by a line or curve is correct and resistant to outliers.

3.2 Cloudy conditions ($F>1$)

The parameterizations of $L\downarrow$ by Idso and Jackson (1969) and Brutsaert (1975) were developed strictly for clear-sky conditions. Following Gabathuler et al. (2001), to accommodate cloudy conditions, we supplemented their equations by adding a cloud factor F in the form of (e.g. Kimball et al., 1982)

$$F(n) = 1 + cn^p \tag{5}$$

where n is cloud cover fraction ($0\leq n\leq 1$), and c and p are coefficients describing cloud characteristics, but are typically chosen as 0.22 and 2, respectively (Sugita and Brutsaert, 1993; Gabathuler et al., 2001).

Konzelmann et al. (1994) developed a cloud factor into their definition of effective emissivity ε_{eff}:

$$\varepsilon_{\text{eff}} = \varepsilon_{cs}(1 - n^p) + \varepsilon_{oc}n^p \tag{6}$$

where ε_{oc} is the atmospheric emissivity during overcast conditions and p is a cloud climatology coefficient fitted to the data. We obtained ε_{oc} using robust fitting techniques

for all overcast (n=1) cases (N=1198).

3.3 Parameterization of cloud cover fraction

Observations of cloud cover, though vital to $L\downarrow$ calculations, are often unavailable in high-latitude glacier environments. Using our data set, we explored the possibility to derive cloud fraction as a function of an atmospheric transmissivity index, τ, given by

$$\tau = \frac{G}{I_{\mathrm{TOA}}} \tag{7}$$

where G is horizontally measured global radiation and I_{TOA} is top of atmosphere radiation. Various functions relating cloud cover fraction n to τ are substituted into Eq. (6) replacing cloud cover fraction as independent variable; the $L\downarrow$ calculations with cloud cover fraction parameterization are then compared to parameterizations with cloud fraction as independent variable for hourly and daily means. Sicart et al. (2006) used an atmospheric transmissivity parameterization similar to this study, although the parameterized cloud emission factor was fitted to atmospheric transmissivity and relative humidity rather than hourly and daily mean cloud fraction. Daily mean cloud cover is largely empirical, based upon identifying 24-h time periods with little or no changes in cloud cover during night hours when observations generally were not, or only sparsely, performed.

3.4 Coefficient fitting and performance evaluation

All three parameterization forms were evaluated for clear-sky, overcast-sky and all-sky conditions by calculating the coefficient of determination (r^2), the root mean square error (RMSE) and the mean bias error (MBE) of the linear regression between measured and computed hourly values. Konzelmann et al. (1994), Greuell et al. (1997) and Klok and Oerlemans (2002) provide varying coefficient values for Eqs. (3) and (6) from fits to their data. Longwave calculations using these coefficients were evaluated

against $L\downarrow$ calculations using coefficients fitted to the Storglaciären data set to assess the potential for coefficient universality.

4 Results

4.1 Clear-sky emissivity calculations and parameterization

Figure 1 shows calculated clear-sky emissivity as a function of the ratio of near-surface vapor pressure to temperature. Hourly clear-sky emissivities tend to scatter around 0.7, a value commonly associated with clear-sky observations and generally consistent with clear-sky emissivities in prior studies (e.g. Konzelmann et al., 1994; Marty and Philipona, 2000). Coefficient fitting of Eq. (4) resulted in b=0.440 and m=8. Values for b in the literature range between 0.407 and 0.484 (Table 1); all fitted clear-sky parameterizations revealed m=8 as the best-fit (Konzelmann et al., 1994; Greuell et al., 1997; Klok and Oerlemans, 2002).

Clear-sky parameterization curves in Fig. 1 give an indication of the sensitivity of parameterized emissivity upon the coefficients used in Eq. (4); too large or too small b resulted in over- or under-represented emissivity values. As expected, the clear-sky emissivity parameterization fitted to our data is most representative of the data; all but 6 calculations fall within the 95th percentile interval of the fitted emissivity parameterization. The theoretically derived Brutsaert (1975) parameterization (no fitting) agrees well with emissivity calculations when the ratio of vapor pressure over temperature is less than ~2.5 Pa/K; above this value clear-sky emissivity becomes over-estimated. Idso and Jackson's (1969) clear-sky emissivity parameterization is not shown since temperature is the only independent variable.

Correlation statistics between clear-sky $L\downarrow$ calculations and measurements are given in Table 1. All but one parameterization resulted in the same coefficient of determination (r^2=0.89), but significant differences in correlation are identified by RMSE and MBE. Table 1 shows RMSEs and MBEs of up to 18 and 17 W m^{-2}, respectively, com-

pared to 7 and 0 W m^{-2} for the case when coefficients are fitted. The Brutsaert (1975) parameterization tends to slightly overestimate $L\downarrow$ (compared to the fitted parameterization), likely due to the over-represented clear-sky emissivity when e_a/T_a is large (Fig. 1). A scatter-plot of clear-sky $L\downarrow$ using the fitted clear-sky parameterization (Eq. 4) is shown in Fig. 2a.

4.2 Overcast-sky emissivity

Equations (1) and (6) (setting n=1) and observations of $L\downarrow$ and T during overcast conditions allowed for linear regression in determining the overcast emissivity coefficient ε_{oc}=0.968; the range of values from the literature is 0.952 to 0.984 (Konzelmann et al., 1994; Greuell et al., 1997; Klok and Oerlemans, 2002). Table 1 lists the fitted and reported coefficient values for the cloud factors. All $L\downarrow$ calculations during overcast conditions resulted in a positive bias, but the fitted overcast emissivity parameterization gave the least positive bias of 4 W m^{-2}; the remaining Konzelmann et al. (1994) overcast parameterizations gave biases between 7 to 10 W m^{-2}. The cloud factor proposed by Kimball et al. (1982), when applied to calculations of $L\downarrow$, is largely inaccurate. RMSE and MBE of 90 W m^{-2} indicate that an emissivity >1 (always occurring for n=1, see Eq. 5) is a systematic error in the development of the cloud factor parameterization.

Almost 85% of overcast $L\downarrow$ calculations from the fitted parameterization are within the 95th percentile intervals of this parameterization (not shown); the remaining 15% suggest large systematic overestimation (up to 90 W m^{-2}) of calculated values (Fig. 2b). A positive systematic bias may be the result of neglecting cloud-base height in the parameterization; cloud-base temperatures of upper-level clouds (above 6–8 km above surface) are significantly lower than low-level clouds, leading to a reduction in emitting blackbody temperature and hence decreased $L\downarrow$ measurements that will not be captured in the parameterization. Differences in cloud optical depth and atmospheric optical depth between the surface and cloud base from low- and upper-level clouds will also influence the effective emissivity. Examination of the cloud levels indicated more

than 75% of the largest outliers in Fig. 2b were calculated during low-level overcast, indicating that high-level cloudiness is not the primary reason for the scatter. Konzelmann et al. (1994) proposed a parameterization using cloud level as independent variable; this parameterization was tested for this study, but an increased correlation between calculations and measurements was not found.

4.3 Comparison of hourly $L\downarrow$ parameterizations under all-sky conditions

A cloud climatology coefficient p describing partial cloudiness characteristics is included in the Konzelmann et al. (1994) effective emissivity Eq. (6). The best-fit for our data set revealed p=2, agreeing with p reported in Greuell et al. (1997) and Klok and Oerlemans (2002). Quantitative results for hourly $L\downarrow$ calculations evaluated with their respective models are given in Table 1. Coefficients of determination (r^2) for all but one model again are nearly identical; instead inter-model comparison of performance is better evaluated by observing RMSE and MBE. The latter varies between −14 and 7 W m^{-2} for all parameterizations, the former between 18 and 23 W m^{-2}.

Systematic biases for each parameterization are apparent in Fig. 3a. Differences between calculated and observed values averaged over 5 W m^{-2} bins reach up to 25 W m^{-2}; differences between the different parameterizations are of the same magnitude indicating large differences between parameterizations. The two models (Idso and Jackson, 1969; Brutsaert, 1975) to which the cloud factor proposed by Kimball et al. (1982) was added have strongest negative biases during large observed $L\downarrow$. For observed $L\downarrow$<280 W m^{-2} (clear to mostly-clear conditions), there is a tendency for the parameterization to overestimate $L\downarrow$, while for larger $L\downarrow$ there is a reverse in $L\downarrow$ bias. Those parameterizations which perform relatively well under mostly clear-sky conditions show largest underestimation under cloudy conditions, while those which have small biases under the latter conditions, yield strongest overestimations under mostly clear skies. The parameterization by Konzelmann et al. (1994) also overestimates low $L\downarrow$ and underestimates high $L\downarrow$, but it has smallest RMSE and MBE (Table 1), and has been chosen as the model with coefficient values fitted to our dataset for use in the next

section. A scatter-plot of calculated and measured $L\downarrow$ using the fitted Storglaciären parameterization is shown in Fig. 3b.

4.4 Cloud cover parameterization

Hourly observations reveal a highly scattered relationship between cloud fraction and atmospheric transmissivity index, τ (Fig. 4a). A large scatter during partially cloudy conditions ($0.2 \leq n \leq 0.8$) is, in part, expected due to difficulty in manual observations of partially cloudy skies. But a significant spread in τ for both clear and especially overcast conditions is also seen, the latter to be expected due to largely varying cloud heights and properties for identical cloud fraction, n. A number of factors such as systematic cloud fraction observation error, aerosol scattering and absorption and varying cloud and atmospheric optical depth can potentially be responsible for the generally large scatter. Use of a digital terrain model to evaluate the likelihood of shading on the PIR sensor may also bias this relationship.

Errors can also stem from using τ as a proxy for cloud cover, as large amounts of high cirrus clouds can effectively give the same transmissivity as broken low-level stratus. The variance of $L\downarrow$ measured during high- and low-level cloud cases was examined, and the variability of both was similar and of the same order of magnitude; the similarity in variance suggests that differences in cloud levels is not the primary source of uncertainty when using atmospheric transmissivity as cloud proxy.

Four different cloud parameterizations were fitted to the data; the equation forms and respective best-fit coefficients are provided in Table 2. Parameterized cloud fraction was set to 0 if calculated values were less than 0, and to 1 if they exceeded 1. With the exception of the linear cloud parameterization, correlation coefficient values are rather large and similar for both hourly and daily averages (Table 2).

When the cloud parameterizations are plotted with the data (Fig. 4a, b), it becomes clear that the large r^2 values primarily come from the relationship between data and parameterizations during clear or overcast skies. However a systematic underestimation will occur for overcast conditions when τ becomes large; clear-sky observations

will be most accurately parameterized, although the parameterization is less than ideal. Parameterizations generally perform the worst during partially cloudy conditions. The cloud parameterizations fare slightly better with the daily mean values; this is likely a caveat to a lack of sufficient data, especially during partial cloudiness (Fig. 4b).

4.5 $L\downarrow$ calculations using cloud parameterization

Each cloud parameterization (Table 2) was substituted for cloud fraction n in the Konzelmann et al. (1994) effective emissivity parameterization Eq. (6); clear-sky emissivity calculations were obtained using the fitted ε_{cs} parameterization. Correlation statistics using the cloud parameterizations are presented in Table 2.

Coefficients of determination, r^2, RMSE and MBE of $L\downarrow$ calculations are within the same range as, and sometimes even better, than those computed when cloud fraction was taken from the observations (Tables 1 and 2). Figure 5a shows mean error in hourly $L\downarrow$ calculations as a function of measured $L\downarrow$; the four lines represent different functions for parameterizing cloud fraction, n. Systematic biases are apparent especially for the linear parameterization. The same systematic biases when cloud fraction was input into the parameterizations re-appear; clear-sky $L\downarrow$ is over-predicted and overcast $L\downarrow$ tends to be under-predicted with a transition between systematic biases near 300 W m^{-2}. The same systematic biases along with similar correlation statistics indicates that the cloud parameterizations developed here are able to predict $L\downarrow$ to the same accuracy as using observed cloud fraction as input.

The three non-linear cloud parameterizations have nearly the same mean $L\downarrow$ errors, especially during clear and partly cloudy conditions. Cubic- and power-form cloud parameterizations resulted in nearly identical hourly calculations and systematic biases as those obtained from using observed cloud fraction. This is an encouraging result which requires additional testing on independent data sets. Calculation of $L\downarrow$ using the power-form cloud parameterization is shown as a scatter-plot in Fig. 5c.

Results from daily mean $L\downarrow$ calculations using the cloud parameterizations are also presented in Table 2. Quantitatively, one sees a strengthened relationship to the ob-

served values; r^2 values have increased by ~12% and RMSE have dropped by 3–4 W m^{-2} in comparison to hourly values.

Daily biases as a function of measured $L\downarrow$ are shown in Fig. 5b. A lack of daily mean observations results in a spiky plot in mean $L\downarrow$ error, but biases are still distinguishable. All parameterizations now lead to an overall negative bias and systematically underestimate $L\downarrow$; only the cubic- and power-form cloud parameterizations show a bias near zero or slightly larger than zero during partial cloudiness. As atmospheric emissivity increases and measured mean $L\downarrow$ increases, the non-linear cloud parameterizations result in calculation errors that are comparable to the hourly $L\downarrow$ parameterization results, both with and without cloud fraction as independent variable.

Calculations made with the cubic- and power-forms yield very similar results, comparable to what was also seen for the hourly calculations. Slightly lower atmospheric emissivity for the quadratic-form parameterization compared to the cubic- and power-form cloud parameterizations (Fig. 4b) results in smaller $L\downarrow$ calculations during partially cloudy conditions. Daily $L\downarrow$ calculations using the power-form cloud parameterization are shown as a scatter-plot in Fig. 5d, illustrating the systematic bias especially during clear-sky conditions. Sicart et al. (2006) also report a strengthened correlation between calculations and measurements for daily values. Systematic biases lead to underestimated $L\downarrow$ using our cloud parameterization, opposite of what is reported by Sicart et al. (2006). The overall RMSE for both hourly and daily calculations is noticeably lower for our parameterization which is based on cloud fraction compared to Sicart et al. (2006) whom rely only on relative humidity.

Overall, results indicate that use of the proposed cloud parameterization yields comparable results to use of cloud fraction observations when parameterizing longwave incoming radiation as a function of cloud cover. The major drawback to using an atmospheric transmissivity parameterization is that global radiation measurements go to zero during hours of darkness. However manual cloud observations are, for the most part, also restricted to daylight hours.

5 Conclusions

Accuracy of $L\downarrow$ calculations using commonly applied parameterizations in the glacier environment have been tested against measurements obtained during multiple melt seasons on Storglaciären in Northern Sweden. The purpose of this examination was to first test the validity of both theoretical and empirical $L\downarrow$ parameterizations as they exist within the literature (including variations of coefficients). A secondary task included an attempt to determine the accuracy of such $L\downarrow$ parameterizations when an additional parameterization for cloud cover is developed and incorporated into the calculations.

Coefficient fitting to the hourly Storglaciären data gave coefficients that agree with the range of coefficient values reported in the literature. Results showed that the relationship between measured and calculated $L\downarrow$ is strengthened using fitted coefficients for clear-, overcast- and all-sky conditions; longwave radiation parameterizations can be used universally but coefficients must be fitted to the data for the most realistic $L\downarrow$ calculations.

The parameterization solely based on air temperature performed worse than those including humidity as well. Although correlation coefficients were similar for the latter, systematic biases varied depending on the parameterization equation applied and coefficient values used. RMSE and MBE worsened by roughly 5 and 13 $\mathrm{W\,m^{-2}}$, respectively between the fitted parameterization and Brutsaert's (1975) commonly used parameterization with the addition of a cloud factor. The general tendency for all parameterizations was overestimation of $L\downarrow$ during clear/mostly-clear skies and underestimation when cloud cover increases. However biases vary significantly depending on parameterization and coefficient values.

Since cloud cover observations often are unavailable we developed a parameterization of cloud cover based on an atmospheric transmissivity index defined as the ratio of global radiation and top of atmosphere radiation, τ. Although there was a large scatter between observed cloud fraction and τ, using parameterized cloud cover in the calculation of longwave incoming radiation revealed nearly identical correlation statistics and

systematic biases as when cloud fraction observations were used. This is promising for longwave radiation modelling in areas where global radiation data are available but cloud observations are not.

References

Aase, J. K. and Idso, S. B.: A Comparison of Two Formula Types for Calculating Long-Wave Radiation From the Atmosphere, Water Resour. Res., 14, 623–625, 1978.

Ångström, A.: Über die Gegenstrahlung der Atmosphäre, Meteorol. Z., 33, 529–538, 1916.

Brunt, D.: Notes on radiation in the atmosphere, Q. J. Roy. Meteorol. Soc., 58, 389–418, 1932.

Brutsaert, W.: On a Derivable Formula for Long-Wave Radiation From Clear Skies, Water Resour. Res., 11, 742–744, 1975.

Gabuthuler, M., Marty, C. and Hanselmann, K. W.: Parameterization of incoming longwave radiation in high-mountain environments, Phys. Geogr., 22, 99–114, 2001.

Greuell, W., Knap, W. H., and Smeets, P. C.: Elevational changes in meteorological variables along a midlatitude glacier during summer, J. Geophys. Res-Atmos., 102(D22), 25 941–25 954, 1997.

Hoch, S. W., Calanca, P., Philipona, R., and Ohmura, A.: Year-round observation of longwave radiative flux divergence in Greenland, J. Appl. Meteorol. Clim., 46(9), 1469–1479, 2007.

Hock, R., Carrivick, J. L., and Jonsell, U.: Glacio-Meteorological Studies On Storglaciären In 1999, Tarfala Research Station – Annual Report 1998–99, Department of Physical Geography, Stockholm University, 20–23, 1999.

Hock, R. and Holmgren, B.: A distributed surface energy-balance model for complex topography and its application to Storglaciären, Sweden, J. Glaciol., 51, 25–36, 2005.

Idso, S. B. and Jackson, R. D.: Thermal radiation from the atmosphere, J. Geophys. Res., 74, 5397–5403, 1969.

Iziomon, M. G., Mayer, H. and Matzarakis, A.: Downward atmospheric longwave irradiance under clear and cloudy skies: Measurement and parameterization, J. Atmos. Sol-Terr. Phy., 65, 1107–1116, 2003.

Kimball, B. A., Idso, S. B., and Aase, J. K.: A model of thermal radiation from partly cloudy and overcast skies, Water Resour. Res., 18, 931–936, 1982.

Klok, E. J. and Oerlemans, J.: Model study of the spatial distribution of the energy and mass balance of Morteratschgletscher, Switzerland, J. Glaciol., 48, 505–518, 2002.
Koenig-Lango, G. and Augstein, F.: Parameterization of the downward long-wave radiation at the Earths surface in polar regions, Meteorol. Z., 3, 343–347, 1994.
Konzelmann, T., van de Wal, R. S. W., Greuell, W., Bintanja, R., Henneken, E. A. C., and Abe-Ouchi, A.: Parameterization of global and longwave incoming radiation for the Greenland Ice Sheet, Global Planet. Change, 9, 143–164, 1994.
Marty, C. and Philipona, R.: The Clear-Sky Index to separate Clear-Sky from Cloudy-Sky Situations in Climate Research, J. Geophys. Res., 27, 2649–2652, 2000.
Marty, C., Philipona, R., Fröhlich, C., and Ohmura, A.: Altitude dependence of surface radiation fluxes and cloud forcing in the Alps: Results from the alpine surface budget network, Theor. Appl. Climatol., 72, 137–155, 2002.
Müller, H.: Review paper: On the radiation budget in the Alps., J. Climatol., 5, 445–462, 1985.
Ohmura, A.: Physical Basis for the Temperature-Based Melt-Index Model, J. Appl. Meteorol., 40, 753–761, 2001.
Philipona, R., Fröhlich, C., and Betz, C.: Characterization of pyrgeometers and the accuracy of atmospheric long-wave radiation measurements, Appl. Optics, 34, 1598–1605, 1995.
Philipona, R., Dürr, B., Marty, C., Ohmura, A., and Wild, M.: Radiative forcing – measured at Earth's surface – corroborate the increasing greenhouse effect, J. Geophys. Res., 31(N3), L03202, doi:10.1029/2003GL018765, 2004.
Pirazzini, R., Nardino, M., Orsini, A., Calzolari, F., Georgiadis, T., and Levizzani, V.: Parameterization of the downward longwave radiation from clear and cloudy skies at Ny Ålesund (Svalbard), in: IRS 2000: Current Problems in Atmospheric Radiation, edited by: Smith, W. L. and Timofeyev, Y. M., A. Deepack Publishing, Hampton, Virginia, 559–562, 2001.
Plüss, C. and Ohmura, A.: Longwave Radiation on Snow-Covered Mountainous Surfaces, J. Appl. Meteorol., 36, 818–824, 1997.
Radic, V. and Hock, R.: Modeling future glacier mass balance and volume changes using ERA-40 reanalysis and climate models: A sensitivity study at Storglaciären, Sweden, J. Geophys. Res., 111, F03003, doi:10.1029/2005JF000440, 2006.
Sicart, J. E., Wagnon, P., and Ribstein, P.: Atmospheric controls of the heat balance of Zongo Glacier (16° S, Bolivia), J. Geophys. Res., 110, D12106, doi:10.1029/2004JD005732, 2005.
Sicart, J. E., Pomeroy, J. W., Essery, R. L. H., and Bewley, D.: Incoming longwave radiation to melting snow: observations, sensitivity and estimation in northern environments, Hydrol.

Processes, 20, 3697–3708, 2006.
Sugita, M. and Brutsaert, W.: Cloud Effect in the Estimation of Instantaneous Downward Longwave Radiation, Water Resour. Res., 29, 599–605, 1993.
Swinbank, W. C.: Long-wave radiation from clear skies, Q. J. Roy. Meteorol. Soc., 89, 330–348, 1963.
Unsworth, M. H. and Monteith, J. L.: Geometry of long-wave radiation at the ground. I. Angular distribution of incoming radiation, Q. J. Roy. Meteorol. Soc., 101, 13–24, 1975.
van den Broeke, M. R.: Characteristics of the lower ablation zone of the west Greenland ice sheet for energy-balance modelling, Ann. Glaciol., 23, 160–166, 1996.
van den Broeke, M. R., Reijmer, C. H., and van de Wal, R. S. W.: The surface radiation balance in Antarctica as measured with Automatic Weather Stations, J. Geophys. Res., 109, D09103, doi:10.1029/2003JD004394, 2004.
van de Wal, R. S. W., Greuell, W., van den Broeke, M. R., Reijmer, C. J., and Oerlemans, J.: Surface mass-balance observations and automatic weather station data along a transect near Kangerlussuaq, West Greenland, Ann. Glaciol., 42, 311–316, 2005.
Yamannouchi, T. and Kawaguchi, S.: Longwave radiation balance under a strong surface inversion in the katabatic wind zone, Antarctica, J. Geophys. Res., 89(D7), 11 771–11 778, 1984.
Zuo, Z. and Oerlemans, J.: Modelling albedo and specific balance of the Greenland ice sheet: calculations for the Søndre Strømfjord transect, J. Glaciol., 42, 305–333, 1996.

Table 1. Parameterization equations comprising the incoming longwave radiation Eq. (1). Three clear-sky emissivity parameterizations Eqs. (2–4) and two cloud factor parameterizations Eqs. (5) and (6) and the respective coefficients values are given. Clear-sky emissivity and cloud factor parameterization developed by Konzelmann et al. (1994) is tested five times due to varying coefficient values found in the literature. Location and time periods of the respective studies are given. Parameterization performance as compared to measurements is given by coefficient of determination (r^2), root mean square error (RMSE) and mean bias error (MBE); these statistics are split into 3 categories: 1) clear-sky conditions, 2) overcast-sky conditions and 3) all-sky conditions.

			Clear-sky			Overcast-sky			All-sky		
Clear sky parameterization (ε_{cs})	Study site/Period	Cloud factor (F)	r^2	RMSE ($W\,m^{-2}$)	MBE ($W\,m^{-2}$)	r^2	RMSE ($W\,m^{-2}$)	MBE ($W\,m^{-2}$)	r^2	RMSE ($W\,m^{-2}$)	MBE ($W\,m^{-2}$)
Eq. (4) Present study b=0.440, m=8	Storglaciären, Sweden 1998–2000, 2002 melt seasons	Eq. (6) Konzelmann et al. (1994) ε_{oc}=0.968, p=2	0.89	6.6	−0.3	0.41	16.4	4.3	0.76	18.0	0.8
Eq. (2) Idso and Jackson (1969)	Theoretically developed	Eq. (5) Kimball et al. (1982) c=0.22, p=2	0.83	11.0	6.2	0.41	91.1	90.0	0.71	22.0	−9.0
Eq. (3) Brutsaert (1975) k=0.642, m=7	Theoretically developed	Eq. (5) Kimball et al. (1982) c=0.22, p=2	0.89	7.3	1.5	0.41	91.1	90.0	0.75	23.0	−14.0
Eq. (4) Konzelmann et al. (1994) b=0.484, m=8	Greenland ice sheet 1990–1991 melt seasons	Eq. (6) Konzelmann et al. (1994) ε_{oc}=0.952, p=4	0.89	18.1	17.0	0.41	19.0	9.7	0.73	19.0	−1.2
Eq. (4) Greuell et al. (1997) – 1 b=0.475, m=8	Pasterze, Austria (2310 m a.s.l.) 1994 melt season	Eq. (6) Konzelmann et al. (1994) ε_{oc}=0.976, p=2	0.89	15.0	13.3	0.41	17.3	7.0	0.77	19.0	7.0
Eq. (4) Greuell et al. (1997) – 2 b=0.407, m=8	Pasterze, Austria (3225 m a.s.l.) 1994 melt season	Eq. (6) Konzelmann et al. (1994) ε_{oc}=0.976, p=2	0.89	15.0	−13.1	0.41	17.3	7.0	0.76	20.3	−1.5
Eq. (4) Klok and Oerlemans (2002) b=0.433, m=8	Morteratschgletscher, Switzerland 1999–2000	Eq. (6) Konzelmann et al. (1994) ε_{oc}=0.984, p=2	0.89	7.3	−3.0	0.41	19.0	10.0	0.76	19.3	4.0

Table 2. Cloud parameterization equations including coefficients determined by the relationship between cloud fraction n and atmospheric transmissivity index τ (Eq. 7) for hourly and daily mean values. The $L\downarrow$ calculation statistics refer to the correlation between observations and calculated longwave incoming radiation $L\downarrow$ when cloud fraction is parameterized instead of taken from the observations.

	Hourly data						Daily data					
	Cloud parameterization statistics			$L\downarrow$ calculation statistics			Cloud parameterization statistics			$L\downarrow$ calculation statistics		
Cloud parameterization	Coefficients	r^2	RMSE	r^2	RMSE ($W\,m^{-2}$)	MBE ($W\,m^{-2}$)	Coefficients	r^2	RMSE	r^2	RMSE ($W\,m^{-2}$)	MBE ($W\,m^{-2}$)
1. $f(\tau)=a_1 \quad \tau+b_1$ "Linear"	$a_1=-1.092$ $b_1=1.204$	0.54	0.2	0.73	20.0	−7.0	$a_1=-1.224$ $b_1=1.226$	0.63	0.2	0.83	16.1	−9.0
2. $f(x)=a_2 \quad \tau^2+b_2 \quad \tau+c_2$ "Quadratic"	$a_2=-2.661$ $b_2=1.095$ $c_2=0.900$	0.86	0.1	0.76	18.3	−2.1	$a_2=-3.644$ $b_2=1.415$ $c_2=0.879$	0.90	0.1	0.86	15.0	−4.0
3. $f(x)=a_3 \quad \tau^3+b_3 \quad \tau^2+c_3 \quad \tau+d_3$ "Cubic"	$a_3=-3.647$ $b_3=4.485$ $c_3=-0.260$ $d_3=1.003$	0.90	0.1	0.76	18.1	0.1	$a_3=-7.449$ $b_3=1.725$ $c_3=-0.952$ $d_3=1.050$	0.91	0.1	0.86	14.0	−1.0
4. $f(x)=a_4 \quad \tau^{b4}+c_4$ "Power"	$a_4=-2.237$ $b_4=3.789$ $c_4=0.998$	0.89	0.1	0.76	18.0	−0.3	$a_4=-4.901$ $b_4=4.520$ $c_4=0.991$	0.92	0.1	0.86	14.0	−0.3

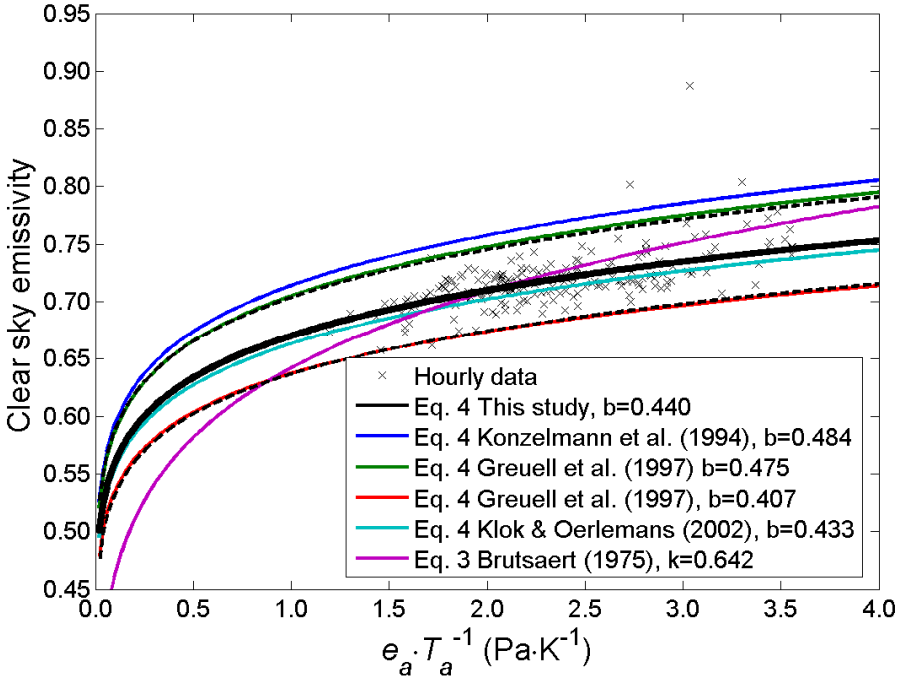

Fig. 1. Clear-sky emissivity versus the ratio of near-surface vapor pressure, e_a, to air temperature, T_a, for all hourly data on Storglaciären with clear-skies (N=205). Clear-sky emissivity parameterizations are shown as solid curves. Equation (4) clear-sky emissivity is parameterized multiple times using the coefficient b fitted to the melt season data on Storglaciären, as well as with values found in the literature over glaciers. Dashed lines represent the bounds of the 95th percentile of the clear-sky emissivity parameterization fitted for this study.

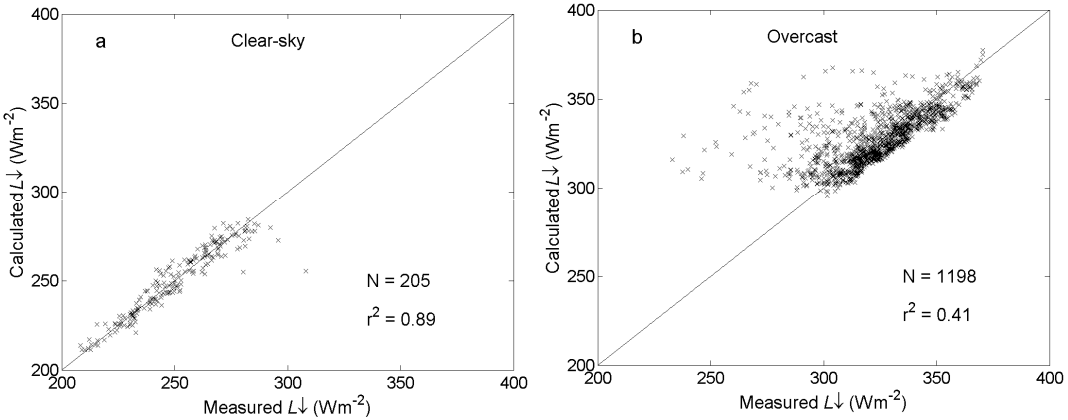

Fig. 2. Calculated versus measured values of hourly incoming longwave radiation $L\downarrow$ computed during **(a)** clear-skies using the fitted clear-sky emissivity parameterization (Eq. 4), and **(b)** overcast-skies using the cloud factor according to Eq. (6) with the fitted overcast emissivity coefficient.

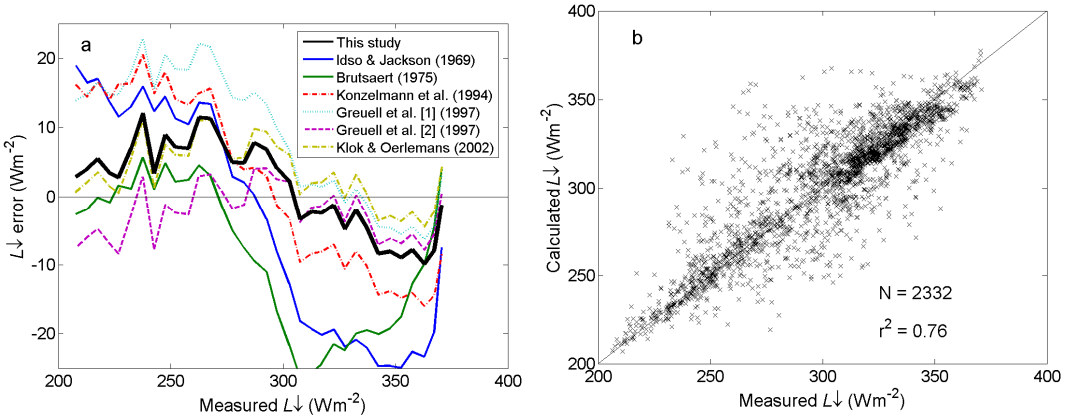

Fig. 3. (a) Hourly error in $L\downarrow$ (here defined as calculated minus measured value) as a function of measured $L\downarrow$ presented as averages over ascending bins of $5\,W\,m^{-2}$. Each line represents a different parameterization and/or different coefficient values comprising Eq. (1); dotted or dashed lines are $L\downarrow$ parameterizations following Konzelmann et al. (1994) for different coefficient values. **(b)** Scatter-plot of calculated vs. measured hourly $L\downarrow$. Calculations are obtained according to Eq. (1) and Eq. (4) using coefficients fitted to our dataset (see Table 1).

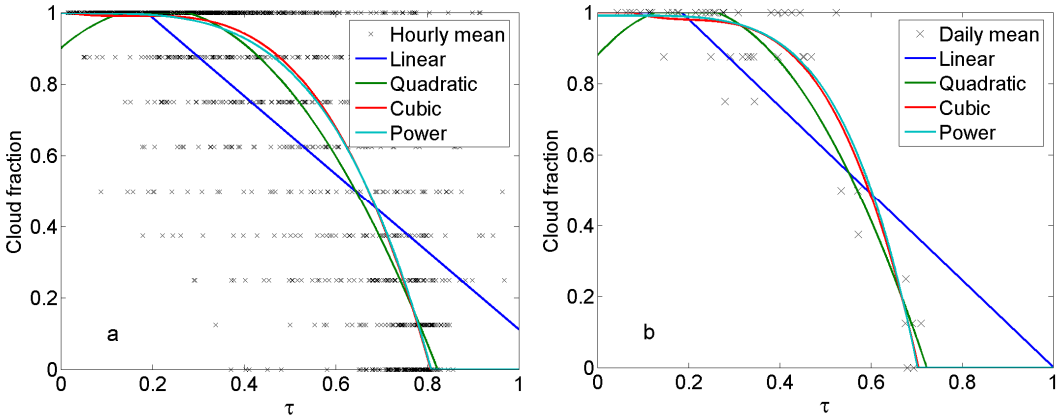

Fig. 4. Cloud fraction as a function of the ratio of measured global radiation and top of atmosphere radiation τ for **(a)** hourly (N=1423) and **(b)** daily (N=51) data. Four cloud parameterization functions, with coefficients robustly fitted to the data, are shown as solid lines (see Table 2 for details).

TCD
2, 487–511, 2008

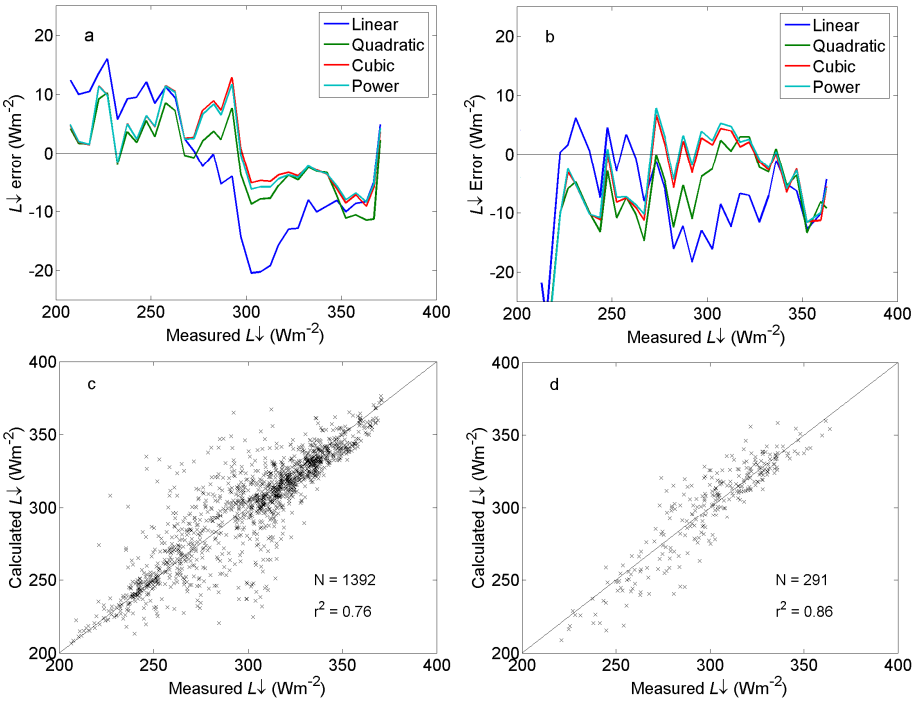

Fig. 5. Same as Fig. 3, except calculations result from the cloud parameterizations based on an atmospheric transmissivity index according to Eq. (7) using four different types of functions fitted to the data (Table 2). **(c)** and **(d)** refer to calculated values using the power-form cloud parameterization for hourly and daily data, respectively.